Facile Synthesis of Ag Nanorods with No Plasmon Resonance Peak in the Visible Region by Using Pd Decahedra of 16 nm in Size as Seeds

Ming Luo,[†,‡] Hongwen Huang,[†] Sang-Il Choi,[†] Chao Zhang,[§] Robson Rosa da Silva,[†] Hsin-Chieh Peng,[⊥] Zhi-Yuan Li,[§] Jingyue Liu,[∥] Zhike He,[‡] and Younan Xia*[,†,⊥]

[†]The Wallace H. Coulter Department of Biomedical Engineering, Georgia Institute of Technology and Emory University, Atlanta, Georgia 30332, United States, [‡]Key Laboratory of Analytical Chemistry for Biology and Medicine, Ministry of Education, College of Chemistry and Molecular Sciences, Wuhan University, Wuhan 430072, P. R. China, [§]Laboratory of Optical Physics, Institute of Physics, Chinese Academy of Science, Beijing 100190, P. R. China, [⊥]School of Chemistry and Biochemistry, School of Chemical and Biomolecular Engineering, Georgia Institute of Technology, Atlanta, Georgia 30332, United States, and [∥]Department of Physics, Arizona State University, Tempe, Arizona 85287, United States

ABSTRACT This article describes a seed-mediated approach to the synthesis of Ag nanorods with thin diameters and tunable aspect ratios. The success of this method is built upon our recent progress in the synthesis of Pd decahedra as uniform samples, together with controllable sizes. When used as a seed, the Pd decahedron could direct the deposition of Ag atoms along the 5-fold axis to generate a nanorod, with its diameter being determined by the lateral dimension of the seed. We were able to generate Ag nanorods with uniform diameters down to 20 nm. Under the conditions we used for growth, symmetry breaking occurred as the Ag atoms were only deposited along one side of the Pd decahedral seed to generate a Ag nanorod with the Pd seed being positioned at one of its two ends. We also systematically investigated the localized surface plasmon resonance (LSPR) properties of the Ag nanorods. With the transverse mode kept below 400 nm, the longitudinal mode could be readily tuned from the visible to the near-infrared region by varying the aspect ratio. As an important demonstration, we obtained Ag nanorods with no LSPR peak in the visible spectrum (400−800 nm), which are attractive for applications related to the fabrication of touchscreen displays, solar films, and energy-saving smart windows.

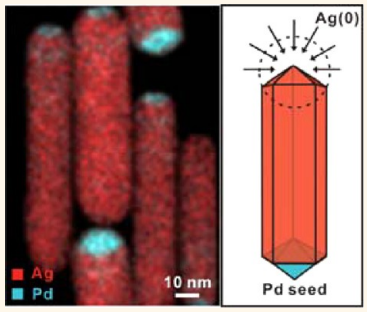

KEYWORDS: silver · nanorods · palladium · seed-mediated growth · galvanic · replacement

Silver nanocrystals have received ever increasing attention as a subject of research because of their great performance in various applications such as catalysis,[1−4] plasmonics,[5−7] surface-enhanced Raman scattering (SERS),[8,9] sensing, imaging,[10] metal-enhanced fluorescence,[11−13] and antimicrobial technology.[14,15] It has been well-established that the physicochemical properties of Ag nanocrystals are strongly correlated with their shapes.[7,16] As a result, tremendous efforts have been devoted to the synthesis of Ag nanocrystals with a myriad of different shapes, including spheres, cubes,[17,18] octahedra,[19,20] cuboctahedra, bipyramids,[21] decahedra,[22] thin plates,[23] bars,[24] rods/wires with a pentagonal cross section,[25−31] and concave structures enclosed by high-index facets.[32] Among them, one-dimensional nanostructures have received particular interest in a number of applications related to the fabrication of conductive and transparent electrodes for touchscreen displays, smart windows, and solar films because of the superior electrical/thermal conductivity of Ag and the tunable localized surface plasmon resonance (LSPR) peaks associated with one-dimensional nanostructures.[33−41]

Nanorods made of coinage metals typically show two distinct LSPR peaks, corresponding to the transverse and longitudinal modes, with their positions being determined by the elemental composition and aspect ratio, respectively.[30,42] For nanorods made of Au and Cu, their transverse peaks are positioned at 520 and 560 nm, respectively,[42−44] making them unfavorable for applications that require high transparency over the entire visible spectrum (400−800 nm).

* Address correspondence to younan.xia@bme.gatech.edu.

Received for review August 13, 2015 and accepted September 15, 2015.

Published online September 15, 2015
10.1021/acsnano.5b05053

TABLE 1. Summary of the Ag Nanorods Synthesized Using Different Types of Seeds

type of seed	smallest diameter[a] (nm)	transverse LSPR peak position (nm)	purity	ref.
Pd decahedra	19.7 ± 2.6	370	>95%	This work
Ag decahedra	49.5 ± 2.5[b]	425	>95%	27
Au decahedra	30 ± 2	393	>98%	30
Au nanorods	15.4 ± 1.7	340–380[c]	>95%	46

[a] Diameter: The definition of "diameter" for a nanorod can be found in Figure S1. [b] Nanorods of 38 nm in diameter were also prepared but their UV–vis spectrum was not reported. [c] The transverse LSPR peak of the Ag nanorods was very broad in the visible region due to the involvement of Au nanorods.

In contrast, the transverse peaks of Ag nanorods can be easily pushed down to wavelengths shorter than 400 nm by reducing their diameters.[7] On the other hand, the longitudinal peaks of Ag nanorods can be readily tuned from the visible to the near-infrared (NIR) region by increasing their aspect ratios. In principle, it is feasible to obtain Ag nanorods with no LSPR peaks in the entire visible spectrum by properly controlling their diameters and aspect ratios.

Seed-mediated growth involving preferential deposition on preformed seeds is probably the most effective approach to the synthesis of Ag nanorods.[25−30,45,46] For nanorods characterized by a pentagonal cross section, decahedral seeds with a 5-fold twinned structure have to be used.[47] To this end, several types of decahedral seeds have been successfully applied to the synthesis of Ag pentagonal nanorods (Table 1). Song and co-workers was among the first in using Au decahedral seeds for the synthesis of Ag nanorods.[26] Following that work, several other groups also explored the use of Au decahedra or Au pentagonal nanorods as seeds to grow Au–Ag bimetallic nanorods.[29,30] In those cases, the nanorods showed broad transverse LSPR peaks in the visible region due to their relatively large diameters. The presence of Au seeds in the nanorods also caused strong absorption in the visible region. To address this issue, Kitaev and co-workers used Ag decahedra as seeds to synthesize Ag nanorods.[27] The Ag nanorods could be prepared with remarkable uniformity and controllable aspect ratios, albeit their transverse LSPR peaks were positioned at wavelengths over 425 nm due to the involvement of relatively large seeds. In addition to the 5-fold twinned seeds, single-crystal Au nanorods have been reported for the preparation of Ag nanorods.[46] In this case, Au@Ag core–shell nanorods were formed through the conformal deposition of Ag shells on Au nanorods. Although the resultant nanorods could be controlled below 20 nm in diameter, their lengths were limited by the Au nanorods. Moreover, the aspect ratio of the core–shell nanorods decreased as the thickness of the Ag shells was increased, resulting in red and blue shifts for the corresponding transverse and longitudinal LSPR modes, respectively. Taken together, the synthesis of Ag nanorods with no LSPR peaks in the entire visible spectrum ranging from 400 to 800 nm remains to be demonstrated.

In the present work, we accomplished the synthesis of Ag nanorods with diameters thinner than 20 nm by taking advantage of recent progress in the synthesis of Pd decahedra with small, controllable sizes. More specifically, our group has developed a robust method for the synthesis of Pd decahedra with controllable sizes down to 6 nm by manipulating the reduction kinetics of a polyol process.[48] The unique features of these newly developed Pd decahedra, including small and controllable sizes, high purity, and good uniformity, make them an excellent candidate for use as seeds in the synthesis of Ag nanorods with small diameters and high purity. Here, we demonstrate that we were able to obtain Ag nanorods with diameters down to 20 nm, while their lengths and thus aspect ratios could be readily tuned by varying the ratio of Ag precursor to Pd decahedral seeds involved in a synthesis. The Ag nanorods with different aspect ratios exhibited remarkably different optical properties. Specifically, their longitudinal LSPR peaks could be tuned from the visible to the NIR region. The use of Pd rather than Au decahedral seeds allowed us to greatly reduce the optical absorption around 520 nm because the LSPR peaks of Pd nanocrystals are typically located in the ultraviolet (UV) region.[49]

RESULTS AND DISCUSSION

Comparison of Different Types of Decahedral Seeds for the Synthesis of Ag Nanorods. Corresponding to light-induced electron oscillations along the short and long axes, respectively, Ag nanorods exhibit transverse and longitudinal LSPR peaks at two different wavelengths.[30] The transverse peak always appears at a wavelength shorter than that of the longitudinal peak. As shown by the extinction spectra calculated using the three-dimensional finite-difference time-domain (3D-FDTD) method (Figure 1A),[50] the position of the transverse LSPR peak was directly proportional to the diameter of the nanorods (see the definition in Figure S1). According to the calculation results, the diameters of the nanorods have to be controlled under 30 nm in order to keep their transverse LSPR peaks below 400 nm. The elemental composition of the decahedral seeds used for the growth of Ag nanorods also has a major impact on the LSPR spectra.[30] As shown in Figure 1B, the LSPR peaks of Au, Ag, and Pd decahedra with the same size of 20 nm (see the definition in Figure S1) were located at very different positions. To avoid strong LSPR in the visible region, one has to avoid the use of Au seeds. Table 1 gives a comparison of the physical parameters of Ag nanorods obtained from different types of decahedral seeds, including the diameters, transverse LSPR peak position, and sample purity. Compared with

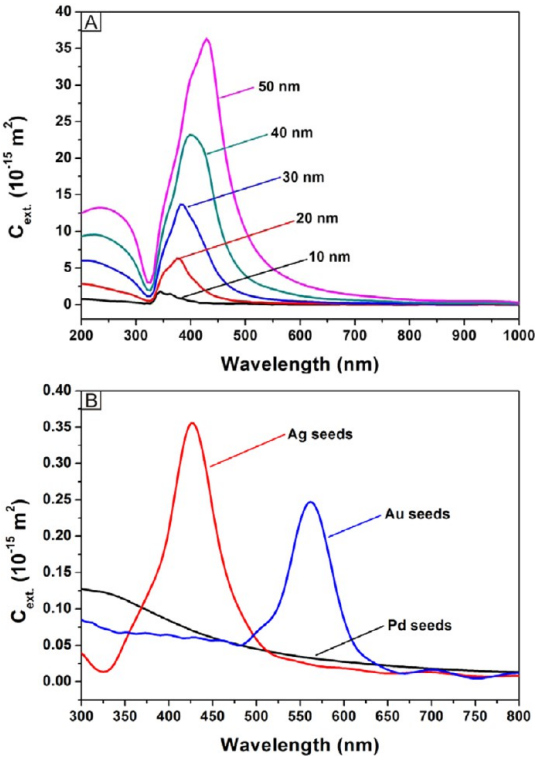

Figure 1. (A) Extinction spectra (transverse mode only) calculated for Ag nanorods with different diameters of 10, 20, 30, 40, and 50 nm by means of the three-dimensional finite-difference time-domain (3D-FDTD) method. The length of the nanorods was fixed at 50 nm. (B) Extinction spectra of decahedral seeds with size of 20 nm made of Ag, Au, and Pd 3D-FDTD calculated.

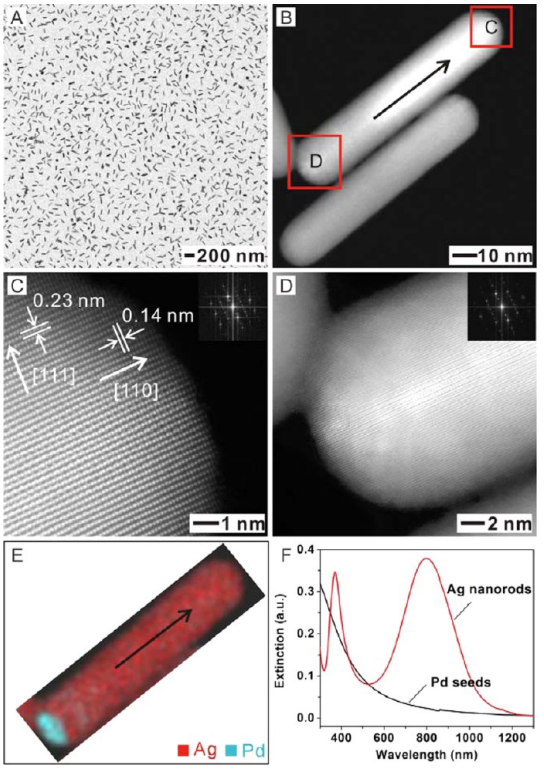

Figure 2. (A) Low-resolution transmission electron microscopy (TEM) and (B) high-angle annular dark-field scanning TEM (HAADF-STEM) image of Ag nanorods grown from 15.8 ± 2.0 nm Pd decahedral seeds. (C and D) High-resolution HAADF-STEM images of the regions boxed in (B). Insets: the corresponding Fourier transform patterns. (E) Energy dispersive X-ray spectroscopy (EDX) mapping of the Ag nanorod shown in (B). (F) The UV−vis-NIR extinction spectra recorded from aqueous suspensions of the Pd decahedral seeds and Ag nanorods synthesized using the standard procedure.

the previous reports, the Ag nanorods prepared in this work offer clear advantages. Owing to the small size of the Pd decahedral seeds, the Ag nanorods reported in this work were much thinner when compared with those grown from either Ag or Au decahedral seeds. More importantly, the Pd decahedral seeds will not contribute any optical absorption to the Ag nanorods in the visible region because their LSPR peak was positioned in the UV region (Figure 1B). As a result, the transverse LSPR peak of the Ag nanorods can be readily pushed down to the UV region to minimize their optical absorption in the visible region.

Synthesis of Ag Nanorods. We used seed-mediated growth to prepare Ag nanorods. The Pd decahedral seeds with a relatively uniform and small size were prepared in high purity using a polyol-based method.[48] Figure S2A shows a transmission electron microscopy (TEM) image of the as-prepared Pd decahedral seeds, which had an average size of 15.8 ± 2.0 nm. Figure S2B shows a typical high-resolution high-angle annular dark-field (HAADF) image recorded from an individual decahedron, which clearly reveals the twin planes characteristic of a decahedron. The lattice spacing of 0.23 nm on the surface of the decahedron can be indexed to the {111} planes of face-centered cubic (fcc) Pd.

In a typical synthesis of Ag nanorods, an ethylene glycol (EG) solution containing specific amounts of $AgNO_3$, poly(diallyldimethylammonium)chloride (PDDA) and the Pd decahedral seeds was magnetically stirred at room temperature. During this process, $AgNO_3$ was converted to AgCl due to the presence of a considerable amount of Cl^- ions released from PDDA. The as-prepared mixture was subsequently heated to 200 °C for 8 h in an oil bath under magnetically stirring. As shown in Figure 2A, the as-obtained product (>95% in purity) was dominated by uniform nanorods with an average length of 76.8 ± 7.4 nm and an average diameter of 19.7 ± 2.6 nm. The definition of "length" and "diameter" for a pentagonal nanorod can be found in Figure S1. Figure 2B shows a HAADF-STEM image of the same sample, confirming the presence of a penta-twinned structure in the nanorod. When the electron-beam was aligned perpendicular to the bottom side of a penta-twinned nanorod (as shown in Figure S3), two sets of fringes with lattice spacing of 0.23 and 0.14 nm were observed (Figure 2C), corresponding to the {111} and {220} planes of Ag, respectively. As shown in Figure 2D, well-defined and continuous {111} fringes (d = 0.23 nm) could be observed in the regions close to

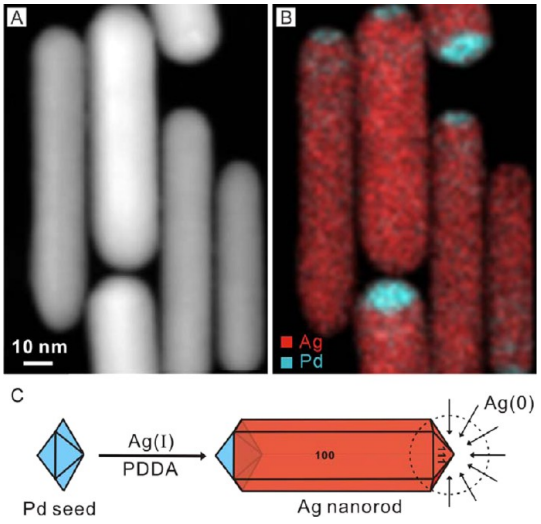

Figure 3. (A and B) HAADF-STEM image and the corresponding EDX mapping of the Ag nanorods. (C) Schematic illustration of a mechanism for the growth of an Ag pentagonal nanorod from one side of a Pd decahedral seed.

the edges of the nanorod, running parallel to the long axis of the nanorod. The brighter fringes with a broader spacing, seen in the central region of the nanorod, could be attributed to double diffraction reflection.[51] The insets in Figure 2C,D give the corresponding Fourier transform patterns, in agreement with the previous results obtained from penta-twinned nanorods made of Ag.[30]

Energy-dispersive X-ray spectroscopy (EDX) mapping was applied to map the distributions of elements in the nanorod. As shown in Figure 2E, the mapping clearly shows an asymmetric distribution of Pd along the Ag nanorod. To further confirm the result, EDX mapping was conducted over a relatively larger area (Figure 3B), showing that all the Pd decahedral seeds were located at one of the two ends of the nanorods. On the basis of the high-resolution HAADF-STEM and EDX mapping analyses, we could conclude that the Ag nanorods had a penta-twinned structure bound by ten {111} facets at two ends and five {100} side faces. The growth of Ag nanorod was along the ⟨110⟩ direction, but only from one side of the Pd decahedral seed (Figure 3C). Figure 2F shows UV−vis-NIR extinction spectra recorded from aqueous suspensions of the Pd decahedral seeds and the Ag nanorods, respectively. The LSPR peak of the Pd decahedral seed was indeed located in the UV region, with essentially no absorption in the visible region. The Ag nanorods with an average aspect ratio of 3.9 exhibited two strong LSPR peaks positioned at 370 and 798 nm, respectively. These two peaks could be assigned to the transverse and longitudinal modes, respectively.

To gain insight into the growth mechanism, we analyzed the products sampled from the reaction solution at different stages of a standard synthesis. Figure 4 shows TEM images of the samples. At t = 1 h (Figure 4A), most of the particles were slightly rounded

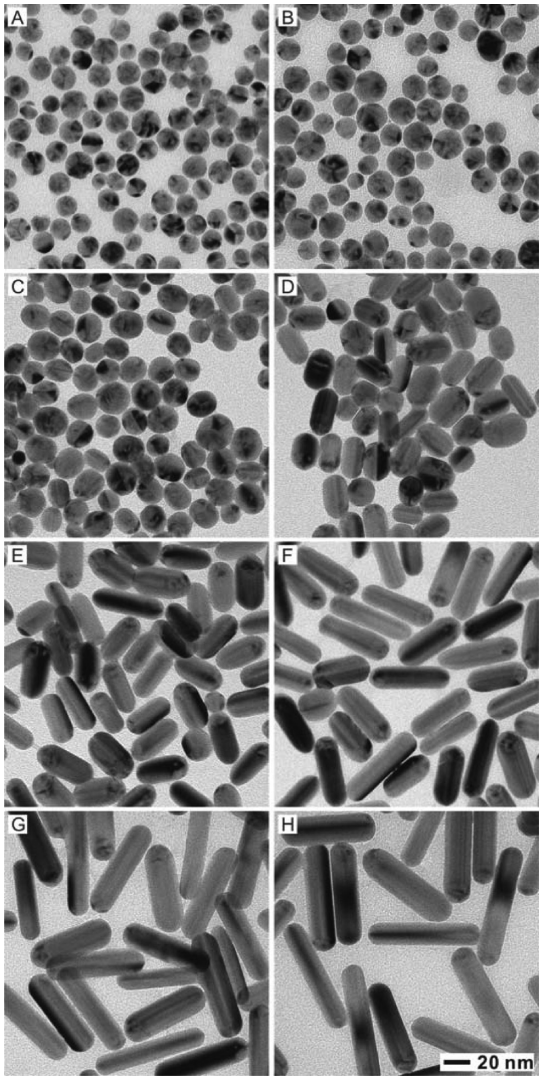

Figure 4. TEM images of the products sampled from a standard synthesis of Ag nanorods after the reaction had proceeded for different periods of time: (A) 1, (B) 2, (C) 3, (D) 4, (E) 5, (F) 6, (G) 7, and (H) 8 h. The scale bar in (H) applies to all other panels.

with an average size of 18.5 ± 2.8 nm, which was a little bit larger than the size of the Pd decahedral seeds. The increase in size can be attributed to the deposition of Ag along the edges of each Pd decahedral seed (Figure S2B).[44] We also noticed that the small Pd seeds disappeared in the sample owing to the involvement of oxidative etching caused by oxygen (from air) and a large amount of Cl^- ions (from PDDA), as well as the use of a relatively high temperature (200 °C).[52] At t = 3 h (Figure 4C), some rod-shaped particles appeared in the product and this demonstrates that the nanostructures started to be elongated along one particular direction. The EDX mapping shown in Figure S4 indicates that almost all the Pd decahedral seeds were located at one of the two ends of the rod-shaped nanoparticles. The aspect ratios of the nanorods then increased to 1.5, 2.0, 2.7, 3.5, and 3.9 as the reaction time was extended to 4, 5, 6, 7, and 8 h, respectively.

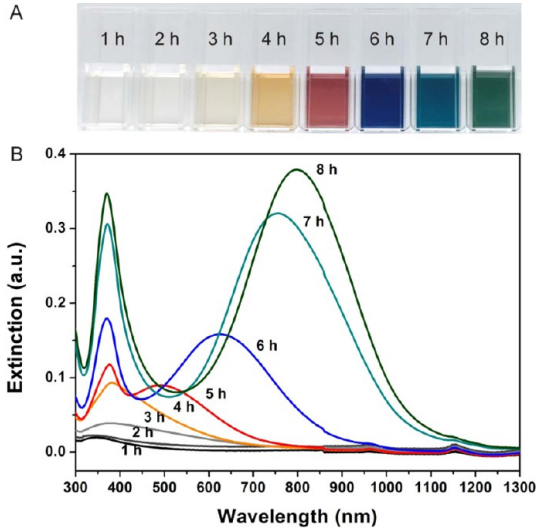

Figure 5. (A) Photograph and (B) the corresponding UV–vis-NIR extinction spectra of the samples as shown in Figure 4.

Figure 5 shows the corresponding photograph and UV–vis-NIR extinction spectra of the products. Accompanying the growth of nanorods, the changes in color were rather striking (Figure 5A). With the increase in length, the color changed from yellow to red, blue, aqua-blue, and green. In the corresponding UV–vis-NIR extinction spectra, the intensities of both the transverse and longitudinal LSPR peaks were enhanced with the increase in reaction time owing to the growth of Ag nanorods. The transverse LSPR peaks were retained at essentially the same position, while the longitudinal peaks were red-shifted to 494, 626, 758, and 798 nm because of the increase in aspect ratio. These results suggest that the length of the Ag nanorods could be easily controlled by terminating the reaction after it had proceeded for a specific period of time when the added amount of Ag precursor was fixed.

As a major advantage of seed-mediated growth, the length of the resultant Ag nanorods could also be readily controlled by varying the ratio between the amounts of Ag precursor and Pd seeds involved in a synthesis. Figure 6 shows TEM images of the Ag nanorods obtained by adding different amounts of $AgNO_3$ into reaction solutions containing the same number of Pd seeds. It can be seen that the aspect ratios of the resultant Ag nanorods increased from 2.1 to 2.6, 3.3, 3.9, 4.4, and 4.9 as the concentration of $AgNO_3$ was increased from 0.1 to 0.2, 0.3, 0.4, 0.5, and 0.6 mM. At a closer look, all of the nanorods displayed fringes in the form of alternating bright and dark stripes known as a Moiré pattern at one of the two ends of a nanorod, revealing the location of the Pd decahedral seed. Figure 7A shows the corresponding UV–vis-NIR spectra recorded from aqueous suspensions of these Ag nanorods. Their transverse LSPR peaks were all located at 370 nm, indicating that the diameters of these Ag nanorods were essentially the same.

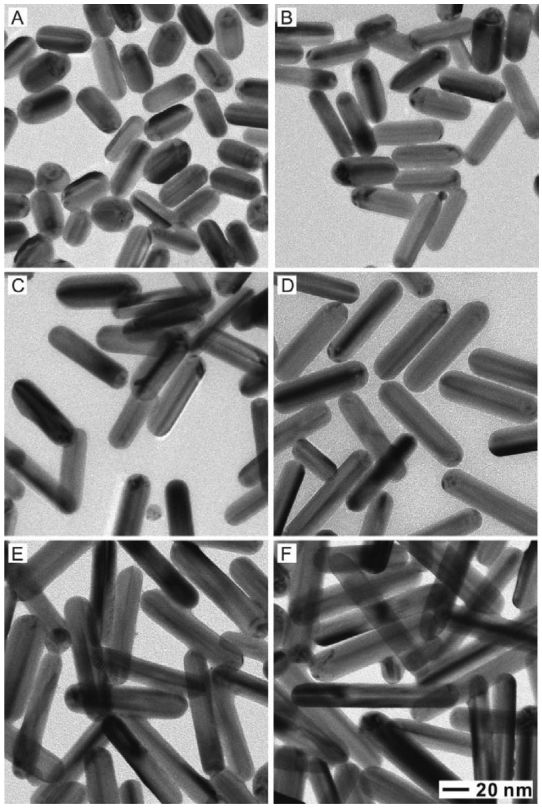

Figure 6. TEM images of the Ag nanorods synthesized at 200 °C using 5 mL of EG solutions containing 20 μg the Pd decahedral seeds, 25 mM PDDA, and $AgNO_3$ in different concentrations: (A) 0.1, (B) 0.2, (C) 0.3, (D) 0.4, (E) 0.5, and (F) 0.6 mM. The scale bar in (F) applies to all other panels.

Their longitudinal LSPR peaks, which are determined by the aspect ratios, were red-shifted from 512 to 598, 702, 798, 890, and 990 nm with the increase in length. Using the 3D-FDTD method,[50] we also calculated the extinction spectra of the Ag nanorods. The calculation results are shown in Figure 7B, which are in qualitative agreement with the experimental data. The discrepancies in both peak width and position could be attributed to the fact that the simulation only involves the use of one nanorod while the nanorods in a real sample can take a relatively broad distribution in terms of length or aspect ratio. Both the experimental and computational results indicate that the longitudinal LSPR peaks of Ag nanorods can be readily tuned into the NIR region.

We further examined the influence of reaction temperature on the morphology of products. In principle, variation of temperature can also be used to adjust the reduction kinetics and thus achieve anisotropic, one-dimensional growth for the decahedral seeds. It is far more challenging, however, to find out the right range of temperature because the reduction rate has an exponential dependence on temperature. In comparison, the reduction rate is linearly proportional to the rate constant (*i.e.*, the combination of precursor and reductant) and the concentrations of reactants. As shown in Figure S5A, decreasing the

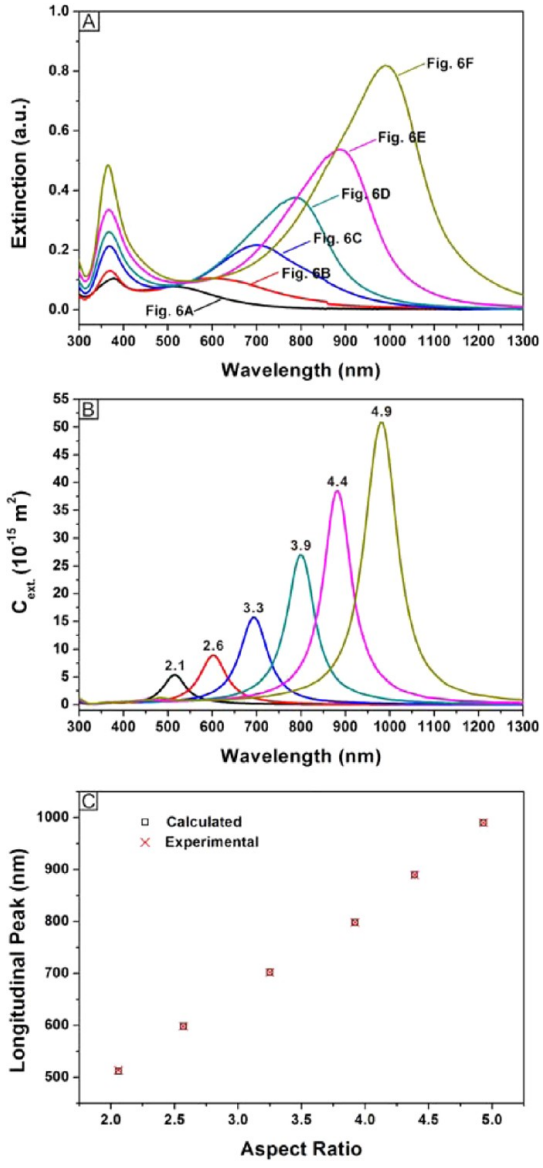

Figure 7. (A) UV−vis-NIR extinction spectra for samples shown in Figure 6A−F. The as-obtained samples of Ag nanorods were diluted by 5 times with DI water prior to spectral measurements. (B) Extinction spectra (the longitudinal mode only) calculated for Ag nanorods with different aspect ratios (labeled on the curves). The diameter of the nanorods was fixed at 20 nm. (C) A plot of the longitudinal LSPR peak position as a function of the aspect ratio.

temperature from 200 to 190 °C, while keeping all other parameters the same as the standard procedure, resulted in shorter nanorods. This change can be attributed to a slower reduction rate at a reduced temperature and thereby a slower growth rate. Longer nanorods, as well as irregular nanoparticles, were observed when the reaction temperature was increased from 200 to 210 °C (Figure S5B), due to the acceleration of growth for the nanorods, as well as possible additional nucleation and growth for the Ag atoms.

Generally, the selective binding of a surfactant to a given crystal plane can significantly slow down the growth rate along the corresponding direction, making that particular plane dominate in the final product. In this synthesis, PDDA plays dual roles in facilitating the formation of Ag nanorods with a pentagonal cross section. On one hand, PDDA provides a considerable amount of Cl^- ions to convert $AgNO_3$ into AgCl. This process is critical to the synthesis as it ensures suitable reduction kinetics for the growth of Ag nanorods. PDDA also helps maintain the Ag atoms at a relatively low concentration to avoid self-nucleation. On the other hand, PDDA can serve as a capping agent for the Ag(100) surface to help control the facets to be developed on the final product.[30] Among various conditions we have examined, PDDA was always needed in order to achieve one-dimensional growth for the Pd decahedral seeds. The impact of PDDA was evaluated by varying the amount of PDDA added into the reaction system. By reducing the concentration of PDDA from 25 to 12.5 mM, Ag nanorods, multiply twinned particles, as well as irregular nanoparticles, were all observed in the products (Figure S5C). The insufficient amount of Cl^- ions in the reaction solution resulted in a faster reduction rate, which could account for the formation of twinned and irregular particles through self-nucleation and growth. When 50 mM of PDDA was employed, pure Ag nanorods were obtained as shown in Figure S5D. On the basis of these observations, it can be concluded that the successful synthesis of Ag nanorods with a penta-twinned structure critically depends on proper reduction kinetics, as mainly controlled by the temperature and concentration of Cl^- ions. As shown in Figure 8, the attenuated total reflectance Fourier transform infrared (ATR-FTIR) spectrum taken from a sample of Ag nanorods (Figure 8B) was essentially identical to that of pure PDDA (Figure 8A). The peaks at 1635 and 1472 cm^{-1}, which could be assigned to C═C vibration, slightly shifted after the reaction (Figure 8B).[53] In addition, two new peaks at 1291 and 880 cm^{-1} appeared in Figure 8B, which could be assigned to N═O and C−N vibrations, respectively.[54] This data suggests that the nitroso group was produced during the synthesis. Combining them together, we can conclude that PDDA molecules in the reaction solution had adsorbed onto the Ag nanorods during the growth process.

The asymmetric growth pattern of Ag on a Pd decahedral seed could be explained using a mechanism we recently reported for symmetry breaking.[55] Although there are multiple, equivalent sites on the surface of a seed, the deposition of newly formed atoms may only occur on some of these available sites when the reduction is too slow to supply a sufficient number of atoms to access all the growth sites. According to our previous reports, the actual growth pattern can be controlled by manipulating the reaction kinetics when Pd nanocubes were used as seeds for the growth of Ag.[55] When the reaction kinetics was slow enough, Ag could only grow along one or a few of the six faces

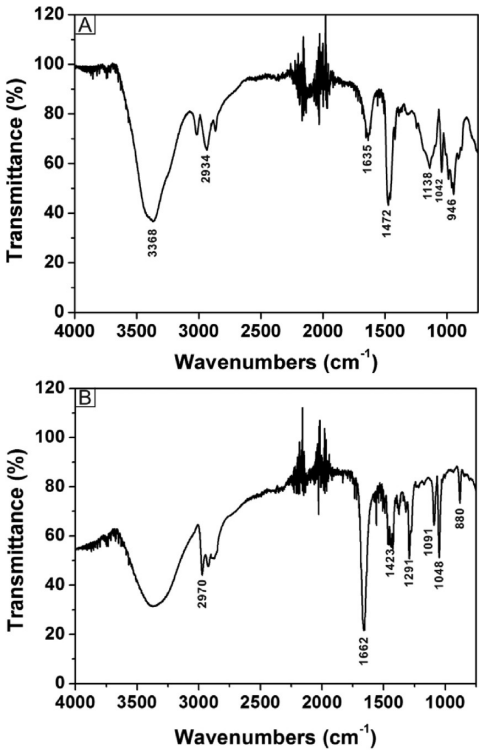

Figure 8. Attenuated total reflectance Fourier transform infrared (ATR-FTIR) spectra taken from (A) pure PDDA and (B) a sample of Ag nanorods (see Figure 2A).

of a cubic Pd seed. This argument is also consistent with what was reported in literature by other groups, where the growth of Ag on Au decahedral seeds could be switched from a symmetric to an asymmetric pattern by slowing down the reaction kinetics.[29] In the present case, the Ag atoms were only deposited on one of the two sides of a Pd decahedral seed due to the slow reduction kinetics caused by PDDA. In addition, the relatively large lattice mismatch (4.5%) between the lattice constants of Ag and Pd could also contribute to the initiation of asymmetric growth.[56]

Synthesis of Au-Based Hollow Nanorods through Galvanic Replacement. Hollow metal nanostructures have attracted ever increasing attention in recent years due to their highly tunable optical properties and great performance in a variety of applications related to catalysis and biomedicine.[57−59] Galvanic replacement has been widely used for the preparation of metallic nanostructures with hollow interiors and porous walls.[60,61] Here, we demonstrate that the galvanic replacement reaction can also be extended to the Ag pentagonal nanorods. Figure S6A shows TEM image of the Au-based hollow structures obtained by adding 5 mL of 0.1 mM $HAuCl_4$ into 5 mL of an aqueous suspension of the Ag nanorods. Clearly, the Au-based hollow structures retained the rod-like morphology of the original Ag nanorods and the Pd decahedral seed was located at one of the two ends, further confirming that the Ag grew from one side of the Pd decahedral seed. As shown in Figure S6B, the Ag nanorods exhibited two major LSPR peaks at 370 nm (the transverse mode) and 500 nm (the longitudinal mode). After galvanic replacement with $HAuCl_4$, The intensities of both the transverse and longitudinal modes associated with the Ag nanorods were dramatically reduced due to the removal of Ag. In comparison with Ag nanorods, the extinction intensity of the hollow structure was increased in the NIR region. Such hollow nanostructures could be promising for various applications related to photothermally triggered drug release, optical imaging, and cancer therapy.

CONCLUSION

We have demonstrated a simple and robust method based on seed-mediated growth for the synthesis of Ag pentagonal nanorods. With the use of Pd decahedral seeds with a size of 15.8 ± 2.0 nm, Ag nanorods with a diameter down to 20 nm were obtained. Their aspect ratios could be readily tuned by varying the amount Ag precursor added into a solution containing a fixed number of Pd decahedral seeds. Structural characterization by TEM, HAADF-STEM, and EDX mapping indicates that the Ag nanorod grew along the ⟨110⟩ direction from one side of the Pd decahedral seed. In this synthesis, PDDA played dual roles: it served as a source of Cl^- ions to regulate the reduction rate of Ag precursor by forming AgCl precipitate and it worked as a capping agent for the Ag(100) surface to facilitate the formation of Ag pentagonal nanorods whose side facets are covered by {111} facets. While the transverse LSPR peak of the Ag nanorods were kept below 400 nm, the longitudinal LSPR peak could be readily tuned into the NIR region by increasing their aspect ratio. In addition, we further demonstrated that the Ag nanorods could be transformed into Au-based hollow nanostructures containing the Pd decahedral seeds at one end *via* the galvanic replacement reaction with $HAuCl_4$. We believe that such Ag nanorods with small diameters and highly tunable LSPR properties will find widespread use in the fabrication of transparent electrodes, touchscreen displays, solar devices, and energy-efficient, smart windows.

EXPERIMENTAL SECTION

Materials. Silver nitrate ($AgNO_3$, 99.8%), sodium tetrachloropalladate(II) (Na_2PdCl_4), sodium sulfate (Na_2SO_4, 99.0%), diethylene glycol (DEG, 99.0%, lot no. BCBJ9535), and poly(diallyldimethylammonium)chloride (PDDA, $M_w \approx$ 400 000−500 000, 20 wt % in water), and poly(vinylpyrrolidone) (PVP, $M_w \approx$ 55 000) were all obtained from Sigma-Aldrich and used as received. Ethylene glycol (EG) was purchased from J. T. Baker. Deionized (DI) water of 18.2 MΩ·cm in resistivity was used throughout the experiments.

Synthesis of Pd Decahedra in DEG. In a typical synthesis of Pd decahedral seeds, 40.0 mg of Na_2SO_4 and 80.0 mg of PVP were dissolved in 2.0 mL of DEG hosted in a 20 mL vial, and the mixture was heated in an oil bath at 105 °C for 20 min under magnetic stirring. Subsequently, 1.0 mL of another DEG solution containing 15.5 mg of Na_2PdCl_4 was added in one shot with a pipet. After the synthesis had proceeded for 24 h, the reaction was quenched by immersing the vial in an ice−water bath. The product was collected by centrifugation at 16 000 rpm and washed once with acetone and then twice with DI water to remove DEG and excess PVP. The Pd decahedra were finally dispersed in EG at a concentration of 1.0 mg/mL, and used as seeds for the synthesis of Ag nanorods.

Synthesis of Ag Nanorods. In a standard synthesis, 20 μL of Pd decahedral seeds was added into 5 mL of EG solution containing 25 mM PDDA, and a specific amount of $AgNO_3$ (as indicated in the figure caption) were introduced into a 20 mL vial. The mixture was magnetically stirred for 15 min at room temperature under ambient conditions. The $AgNO_3$ was quickly converted to AgCl due to the presence of a considerable amount of Cl^- ions released from PDDA. The as-prepared mixture was then subject to heating at 200 °C for 8 h in an oil bath. The final product was collected by centrifugation at 16 000 rpm and washed once with acetone and then twice with DI water to remove residual EG and PDDA. The Ag nanorods were finally dispersed in DI water at a concentration of 1 mg/mL for further use.

Synthesis of Au-Based Hollow Nanorods. In a typical synthesis, 200 μL of the suspension of Ag nanorods was dispersed in 5 mL of aqueous PVP solution (1 mg/mL) and heated to 90 °C under magnetic stirring. Then, 5 mL of aqueous $HAuCl_4$ solution (0.1 mM) was added using a syringe pump at a rate of 5 mL/h. We sampled solutions at different stages of the titration and recorded their UV−vis-NIR extinction spectra to track the progress of the reaction as the volume of $HAuCl_4$ solution was increased. The final solution was cooled down to room temperature and treated with 10 mL of saturated NaCl solution to remove AgCl. The product was collected by centrifugation and washing with DI water three times, and dispersed in DI water for further characterization.

Instrumentation. TEM images were taken using a Hitachi HT7700 microscope operated at 120 kV. HAADF-STEM images were acquired using a JEOL JEM 2200FS STEM microscope equipped with a CEOS probe corrector (Heidelberg, Germany) to provide a nominal image resolution of 0.07 nm. The concentrations of Pd decahedral seeds and Ag nanorods were determined using an inductively coupled plasma mass spectrometer (ICP-MS, NexION 300Q, PerkinElmer). The UV−vis-NIR extinction spectra were recorded on a lambda 750 spectrometer (PerkinElmer). The ATR-FTIR spectra were obtained using a FTIR spectrometer (Varian, 640-IR).

Numerical Simulations. The LSPR extinction spectra of Pd, Ag, Au decahedral seeds and Ag nanorods were simulated using the 3D-FDTD method.[50] In the simulations, the studied region is a $3 \times 3 \times 3\ \mu m^3$ cube, which is surrounded by perfect-matched layers. The scheme of nonuniform meshes was adopted and the size of mesh was 0.5 nm in the middle cubic region of 100 nm in edge length. The long axis of the nanorod was placed along the *x*-axis. All the metal nanoparticles were embedded in water and excited by a plane wave that propagates along the *z*-axis with its electric field polarized along the *x*-axis.

Conflict of Interest: The authors declare no competing financial interest.

Acknowledgment. This work was supported in part by a research grant from NSF (DMR 1506018) and startup funds from the Georgia Institute of Technology. As a jointly supervised Ph.D. candidate from Wuhan University, M.L. was also partially supported by a fellowship from the China Scholarship Council.

Supporting Information Available: The Supporting Information is available free of charge on the ACS Publications website at DOI: 10.1021/acsnano.5b05053

Additional figures (PDF).

REFERENCES AND NOTES

1. Cong, H.; Becker, C. F.; Elliott, S. J.; Grinstaff, M. W.; Porco, J. A., Jr. Silver Nanoparticle-Catalyzed Diels-Alder Cycloadditions of 2′-Hydroxychalcones. *J. Am. Chem. Soc.* **2010**, *132*, 7514–7518.
2. Jiang, Z.-J.; Liu, C.-Y.; Sun, L.-W. Catalytic Properties of Silver Nanoparticles Supported on Silica Spheres. *J. Phys. Chem. B* **2005**, *109*, 1730–1735.
3. Christopher, P.; Linic, S. Engineering Selectivity in Heterogeneous Catalysis: Ag Nanowires as Selective Ethylene Epoxidation Catalysts. *J. Am. Chem. Soc.* **2008**, *130*, 11264–11265.
4. Salehi-Khojin, A.; Jhong, H.-R. M.; Rosen, B. A.; Zhu, W.; Ma, S.; Kenis, P. J. A.; Masel, R. I. Nanoparticle Silver Catalysts That Show Enhanced Activity for Carbon Dioxide Electrolysis. *J. Phys. Chem. C* **2013**, *117*, 1627–1632.
5. Sherry, L. J.; Chang, S.-H.; Schatz, G. C.; Van Duyne, R. P.; Wiley, B. J.; Xia, Y. Localized Surface Plasmon Resonance Spectroscopy of Single Silver Nanocubes. *Nano Lett.* **2005**, *5*, 2034–2038.
6. Sönnichsen, C.; Reinhard, B. M.; Liphardt, J.; Alivisatos, A. P. A Molecular Ruler Based on Plasmon Coupling of Single Gold and Silver Nanoparticles. *Nat. Biotechnol.* **2005**, *23*, 741–745.
7. Rycenga, M.; Cobley, C. M.; Zeng, J.; Li, W.; Moran, C. H.; Zhang, Q.; Qin, D.; Xia, Y. Controlling the Synthesis and Assembly of Silver Nanostructures for Plasmonic Applications. *Chem. Rev.* **2011**, *111*, 3669–3712.
8. Yang, Y.; Liu, J.; Fu, Z.-W.; Qin, D. Galvanic Replacement-Free Deposition of Au on Ag for Core-Shell Nanocubes with Enhanced Chemical Stability and SERS Activity. *J. Am. Chem. Soc.* **2014**, *136*, 8153–8156.
9. Nie, S.; Emory, S. R. Probing Single Molecules and Single Nanoparticles by Surface-Enhanced Raman Scattering. *Science* **1997**, *275*, 1102–1106.
10. Lee, K.-S.; El-Sayed, M. A. Gold and Silver Nanoparticles in Sensing and Imaging: Sensitivity of Plasmon Response to Size, Shape, and Metal Composition. *J. Phys. Chem. B* **2006**, *110*, 19220–19225.
11. Aslan, K.; Gryczynski, I.; Malicka, J.; Matveeva, E.; Lakowicz, J. R.; Geddes, C. D. Metal-Enhanced Fluorescence: An Emerging Tool in Biotechnology. *Curr. Opin. Biotechnol.* **2005**, *16*, 55–62.
12. Zhang, J.; Fu, Y.; Chowdhury, M. H.; Lakowicz, J. R. Metal-Enhanced Single-Molecule Fluorescence on Silver Particle Monomer and Dimer: Coupling Effect between Metal Particles. *Nano Lett.* **2007**, *7*, 2101–2107.
13. Aslan, K.; Wu, M.; Lakowicz, J. R.; Geddes, C. D. Fluorescent Core-Shell Ag@SiO_2 Nanocomposites for Metal-Enhanced Fluorescence and Single Nanoparticle Sensing Platforms. *J. Am. Chem. Soc.* **2007**, *129*, 1524–1525.
14. Kumar, A.; Vemula, P. K.; Ajayan, P. M.; John, G. Silver-Nanoparticle-Embedded Antimicrobial Paints Based on Vegetable Oil. *Nat. Mater.* **2008**, *7*, 236–241.
15. Rai, M. K.; Deshmukh, S. D.; Ingle, A. P.; Gade, A. K. Silver Nanoparticles: the Powerful Nanoweapon against Multidrug-Resistant Bacteria. *J. Appl. Microbiol.* **2012**, *112*, 841–852.
16. Lu, X.; Rycenga, M.; Skrabalak, S. E.; Wiley, B. J.; Xia, Y. Chemical Synthesis of Novel Plasmonic Nanoparticles. *Annu. Rev. Phys. Chem.* **2009**, *60*, 167–192.
17. Zhang, Q.; Li, W.; Moran, C.; Zeng, J.; Chen, J.; Wen, L.-P.; Xia, Y. Seed-Mediated Synthesis of Ag Nanocubes with Controllable Edge Lengths in the Range of 30−200 nm and Comparison of Their Optical Properties. *J. Am. Chem. Soc.* **2010**, *132*, 11372–11378.
18. Wang, Y.; Zheng, Y.; Huang, C.; Xia, Y. Synthesis of Ag Nanocubes 18−32 nm in Edge Length: The Effects of Polyol on Reduction Kinetics, Size Control, and Reproducibility. *J. Am. Chem. Soc.* **2013**, *135*, 1941–1951.
19. Tao, A.; Sinsermsuksakul, P.; Yang, P. Polyhedral Silver Nanocrystals with Distinct Scattering Signatures. *Angew. Chem., Int. Ed.* **2006**, *45*, 4597–4601.
20. Wang, Y.; Wan, D.; Xie, S.; Xia, X.; Huang, C.; Xia, Y. Synthesis of Silver Octahedra with Controlled Sizes and Optical

Properties *via* Seed-Mediated Growth. *ACS Nano* **2013**, *7*, 4586–4594.
21. Wiley, B. J.; Xiong, Y.; Li, Z.-Y.; Yin, Y.; Xia, Y. Right Bipyramids of Silver: A New Shape Derived from Single Twinned Seeds. *Nano Lett.* **2006**, *6*, 765–768.
22. Pietrobon, B.; Kitaev, V. Photochemical Synthesis of Monodisperse Size-Controlled Silver Decahedral Nanoparticles and Their Remarkable Optical Properties. *Chem. Mater.* **2008**, *20*, 5186–5190.
23. Zhang, Q.; Hu, Y.; Guo, S.; Goebl, J.; Yin, Y. Seeded Growth of Uniform Ag Nanoplates with High Aspect Ratio and Widely Tunable Surface Plasmon Bands. *Nano Lett.* **2010**, *10*, 5037–5042.
24. Wiley, B. J.; Chen, Y.; McLellan, J. M.; Xiong, Y.; Li, Z.-Y.; Ginger, D.; Xia, Y. Synthesis and Optical Properties of Silver Nanobars and Nanorice. *Nano Lett.* **2007**, *7*, 1032–1036.
25. Jana, N. R.; Gearheart, L.; Murphy, C. J. Wet Chemical Synthesis of Silver Nanorods and Nanowires of Controllable Aspect Ratio. *Chem. Commun.* **2001**, *24*, 617–618.
26. Seo, D.; Yoo, C. I.; Jung, J.; Song, H. Ag-Au-Ag Heterometallic Nanorods Formed through Directed Anisotropic Growth. *J. Am. Chem. Soc.* **2008**, *130*, 2940–2941.
27. Pietrobon, B.; McEachran, M.; Kitaev, V. Synthesis of Size-Controlled Faceted Pentagonal Silver Nanorods with Tunable Plasmonic Properties and Self-Assembly of These Nanorods. *ACS Nano* **2009**, *3*, 21–26.
28. Zhang, J.; Langille, M. R.; Mirkin, C. A. Synthesis of Silver Nanorods by Low Energy Excitation of Spherical Plasmonic Seeds. *Nano Lett.* **2011**, *11*, 2495–2498.
29. Yang, Y.; Wang, W.; Li, X.; Chen, W.; Fan, N.; Zou, C.; Chen, X.; Xu, X.; Zhang, L.; Huang, S. Controlled Growth of Ag/Au Bimetallic Nanorods through Kinetics Control. *Chem. Mater.* **2013**, *25*, 34–41.
30. Li, C.; Sun, L.; Sun, Y.; Teranishi, T. One-Pot Controllable Synthesis of Au@Ag Heterogeneous Nanorods with Highly Tunable Plasmonic Absorption. *Chem. Mater.* **2013**, *25*, 2580–2590.
31. Sun, Y.; Xia, Y. Large-Scale Synthesis of Uniform Silver Nanowires through a Soft, Self-Seeding, Polyol Process. *Adv. Mater.* **2002**, *14*, 833–837.
32. Xia, X.; Zeng, J.; McDearmon, B.; Zheng, Y.; Li, Q.; Xia, Y. Silver Nanocrystals with Concave Surfaces and Their Optical and Surface-Enhanced Raman Scattering Properties. *Angew. Chem., Int. Ed.* **2011**, *50*, 12542–12546.
33. Hu, L.; Kim, H. S.; Lee, J.-Y.; Peumans, P.; Cui, Y. Scalable Coating and Properties of Transparent, Flexible, Silver Nanowire Electrodes. *ACS Nano* **2010**, *4*, 2955–2963.
34. Hu, L.; Wu, H.; Cui, Y. Metal Nanogrids, Nanowires, and Nanofibers for Transparent Electrodes. *MRS Bull.* **2011**, *36*, 760–765.
35. Tokuno, T.; Nogi, M.; Karakawa, M.; Jiu, J.; Nge, T. T.; Aso, Y.; Suganuma, K. Fabrication of Silver Nanowire Transparent Electrodes at Room Temperature. *Nano Res.* **2011**, *4*, 1215–1222.
36. Langley, D.; Giusti, G.; Mayousse, C.; Celle, C.; Bellet, D.; Simonato, J.-P. Flexible Transparent Conductive Materials Based on Silver Nanowire Networks: A Review. *Nanotechnology* **2013**, *24*, 452001–452020.
37. Wu, H.; Kong, D.; Ruan, Z.; Hsu, P.-C.; Wang, S.; Yu, Z.; Carney, T. J.; Hu, L.; Fan, S.; Cui, Y. Transparent Electrode Based on a Metal Nanotrough Network. *Nat. Nanotechnol.* **2013**, *8*, 421–425.
38. Madaria, A. R.; Kumar, A.; Zhou, C. Large Scale, Highly Conductive and Patterned Transparent Films of Silver Nanowires on Arbitrary Substrates and Their Application in Touch Screens. *Nanotechnology* **2011**, *22*, 245201–245207.
39. Lee, J.; Lee, P.; Lee, H.; Lee, D.; Lee, S. S.; Ko, S. H. Very Long Ag Nanowire Synthesis and Its Application in a Highly Transparent, Conductive and Flexible Metal Electrode Touch Panel. *Nanoscale* **2012**, *4*, 6408–6414.
40. Kang, M.-G.; Xu, T.; Park, H. J.; Luo, X.; Guo, L. J. Efficiency Enhancement of Organic Solar Cells Using Transparent Plasmonic Ag Nanowire Electrodes. *Adv. Mater.* **2010**, *22*, 4378–4383.
41. Leem, D.-S.; Edwards, A.; Faist, M.; Nelson, J.; Bradley, D. D. C.; de Mello, J. C. Efficient Organic Solar Cells with Solution-Processed Silver Nanowire Electrodes. *Adv. Mater.* **2011**, *23*, 4371–4375.
42. Nikoobakht, B.; El-Sayed, M. A. Preparation and Growth Mechanism of Gold Nanorods (NRs) Using Seed-Mediated Growth Method. *Chem. Mater.* **2003**, *15*, 1957–1962.
43. Salzemann, C.; Brioude, A.; Pileni, M.-P. Tuning of Copper Nanocrystals Optical Properties with Their Shapes. *J. Phys. Chem. B* **2006**, *110*, 7208–7212.
44. Zhang, Q.; Zhou, Y.; Villarreal, E.; Lin, Y.; Zou, S.; Wang, H. Faceted Gold Nanorods: Nanocuboids, Convex Nanocuboids, and Concave Nanocuboids. *Nano Lett.* **2015**, *15*, 4161–4169.
45. Zhang, W.; Goh, H. Y. J.; Firdoz, S.; Lu, X. Growth of Au@Ag Core-Shell Penta-twinned Nanorods: Tuning the End Facets. *Chem. - Eur. J.* **2013**, *19*, 12732–12738.
46. Xiang, Y.; Wu, X.; Liu, D.; Li, Z.; Chu, W.; Feng, L.; Zhang, K.; Zhou, W.; Xie, S. Gold Nanorod-Seeded Growth of Silver Nanostructures: From Homogeneous Coating to Anisotropic Coating. *Langmuir* **2008**, *24*, 3465–3470.
47. Huang, H.; Zhang, L.; Lv, T.; Ruditskiy, A.; Liu, J.; Ye, Z.; Xia, Y. Five-Fold Twinned Pd Nanorods and Their Use as Templates for the Synthesis of Bimetallic or Hollow Nanostructures. *ChemNanoMat* **2015**, *1*, 246–252.
48. Huang, H.; Wang, Y.; Ruditskiy, A.; Peng, H.-C.; Zhao, X.; Zhang, L.; Liu, J.; Ye, Z.; Xia, Y. Polyol Syntheses of Palladium Decahedra and Icosahedra as Pure Samples by Maneuvering the Reaction Kinetics with Additives. *ACS Nano* **2014**, *8*, 7041–7050.
49. Xiong, Y.; Chen, J.; Wiley, B. J.; Xia, Y.; Yin, Y.; Li, Z.-Y. Size-Dependence of Surface Plasmon Resonance and Oxidation for Pd Nanocubes Synthesized *via* a Seed Etching Process. *Nano Lett.* **2005**, *5*, 1237–1242.
50. Grimault, A.-S.; Vial, A.; Lamy de la Chapelle, M. Modeling of Regular Gold Nanostructures Arrays for SERS Applications Using a 3D FDTD Method. *Appl. Phys. B: Lasers Opt.* **2006**, *84*, 111–115.
51. Johnson, C. J.; Dujardin, E.; Davis, S. A.; Murphy, C. J.; Mann, S. Growth and Form of Gold Nanorods Prepared by Seed-Mediated, Surfactant-Directed Synthesis. *J. Mater. Chem.* **2002**, *12*, 1765–1770.
52. Xia, Y.; Xiong, Y.; Lim, B.; Skrabalak, S. E. Shape-Controlled Synthesis of Metal Nanocrystals: Simple Chemistry Meets Complex Physics? *Angew. Chem., Int. Ed.* **2009**, *48*, 60–103.
53. Yang, D.-Q.; Rochette, J.-F.; Sacher, E. Spectroscopic Evidence for π-π Interaction between Poly(diallyl dimethylammonium) Chloride and Multiwalled Carbon Nanotubes. *J. Phys. Chem. B* **2005**, *109*, 4481–4484.
54. Chen, H.; Wang, Y.; Dong, S. An Effective Hydrothermal Route for the Synthesis of Multiple PDDA-Protected Noble-Metal Nanostructures. *Inorg. Chem.* **2007**, *46*, 10587–10593.
55. Zhu, C.; Zeng, J.; Tao, J.; Johnson, M. C.; Schmidt-Krey, I.; Blubaugh, L.; Zhu, Y.; Gu, Z.; Xia, Y. Kinetically Controlled Overgrowth of Ag or Au on Pd nanocrystal Seeds: From Hybrid Dimers to Nonconcentric and Concentric Bimetallic Nanocrystals. *J. Am. Chem. Soc.* **2012**, *134*, 15822–15831.
56. Jin, M.; Zhang, H.; Wang, J.; Zhong, X.; Lu, N.; Li, Z.-Y.; Xie, Z.; Kim, M. J.; Xia, Y. Copper Can Still be Epitaxially Deposited on Palladium Nanocrystals to Generate Core-Shell Nanocubes Despite Their Large Lattice Mismatch. *ACS Nano* **2012**, *6*, 2566–2573.
57. Xia, Y.; Li, W.; Cobley, C. M.; Chen, J.; Xia, X.; Zhang, Q.; Yang, M.; Cho, E. C.; Brown, P. K. Gold Nanocages: From Synthesis to Theranostic Applications. *Acc. Chem. Res.* **2011**, *44*, 914–924.
58. Zhang, S.-H.; Xie, Z.-X.; Jiang, Z.-Y.; Xu, X.; Xiang, J.; Huang, R.-B.; Zheng, L.-S. Synthesis of Silver Nanotubes by Electroless Deposition in Porous Anodic Aluminum Oxide Templates. *Chem. Commun.* **2004**, *24*, 1106–1107.
59. Zhang, W.; Rahmani, M.; Niu, W.; Ravaine, S.; Hong, M.; Lu, X. Tuning Interior Nanogaps of Double-Shelled Au/Ag

Nanoboxes for Surface-Enhanced Raman Scattering. *Sci. Rep.* **2015**, *5*, 8382–8387.
60. Seo, D.; Song, H. Asymmetric Hollow Nanorod Formation through a Partial Galvanic Replacement Reaction. *J. Am. Chem. Soc.* **2009**, *131*, 18210–18211.
61. Jing, H.; Wang, H. Structural Evolution of Ag-Pd Bimetallic Nanoparticles through Controlled Galvanic Replacement: Effects of Mild Reducing Agents. *Chem. Mater.* **2015**, *27*, 2172–2180.